NOTICE OF COPYRIGHT This manuscript has been authored by UT-Battelle, LLC under Contract No. DE-AC05-00OR22725 with the U.S. Department of Energy. The United States Government retains and the publisher, by accepting the article for publication, acknowledges that the United States Government retains a non-exclusive, paid-up, irrevocable, world-wide license to publish or reproduce the published form of this manuscript, or allow others to do so, for United States Government purposes. The Department of Energy will provide public access to these results of federally sponsored research in accordance with the DOE Public Access Plan (http://energy.gov/downloads/doe-public-access-plan).

arXiv:1701.07971v2 [cond-mat.str-el] 21 Mar 2017

Role of Quantum Fluctuations in $Ba_3CoSb_2O_9$ Revealed by Excitations within the 1/3-Magnetization Plateau

Y. Kamiya,[1,*] L. Ge,[2] Tao Hong,[3] Y. Qiu,[4] D. L. Quintero-Castro,[5] H. B. Cao,[3]
M. Matsuda,[3] C. D. Batista,[6,7] M. Mourigal,[2] H. D. Zhou,[6,8] and J. Ma[9,10,6,†]

[1]*Condensed Matter Theory Laboratory, RIKEN, Wako, Saitama 351-0198, Japan*
[2]*School of Physics, Georgia Institute of Technology, Atlanta, GA 30332, USA*
[3]*Quantum Condensed Matter Division, Oak Ridge National Laboratory, Oak Ridge, Tennessee 37831, USA*
[4]*NIST Centre for Neutron Research, National Institute of Standards and Technology, Gaithersburg, MD 20899, USA*
[5]*Helmholtz-Zentrum Berlin für Materialien und Energie, D-14109 Berlin, Germany*
[6]*Department of Physics and Astronomy, University of Tennessee, Knoxville, Tennessee 37996, USA*
[7]*Quantum Condensed Matter Division and Shull-Wollan Center, Oak Ridge National Laboratory, Oak Ridge, Tennessee 37831, USA*
[8]*National High Magnetic Field Laboratory, Florida State University, Tallahassee, FL 32310, USA*
[9]*Key Laboratory of Artificial Structures and Quantum Control, Department of Physics and Astronomy, Shanghai Jiao Tong University, Shanghai 200240, China*
[10]*Collaborative Innovation Center of Advanced Microstructures, Nanjing, Jiangsu 210093, China*

(Dated: March 22, 2017)

A recent experiment revealed that the spin-1/2 triangular-lattice Heisenberg antiferromagnet $Ba_3CoSb_2O_9$ is a magnetically ordered material with an anomalous excitation spectrum, comprising a high-intensity excitation continuum and short-lived magnons, which cannot be explained with spin wave theory [Ma *et al.*, Phys. Rev. Lett. **116**, 087201 (2016)]. We use neutron scattering measurements in high magnetic field to map the magnetic excitations of $Ba_3CoSb_2O_9$ in its 1/3-magnetization plateau, which enables an investigation on the precise role of quantum fluctuations. The measured excitation spectrum of the up-up-down phase induced by a magnetic field of $\gtrsim 9.8\,\mathrm{T}$ is quantitatively explained by nonlinear spin wave theory, confirming the validity of the spin Hamiltonian previously obtained for this material. Most importantly, our new findings indicate that the anomalous zero-field spin dynamics has an intrinsic quantum mechanical origin.

Highly frustrated quantum magnets [1] currently offer the main venue in the search for quantum spin liquids (QSLs), along with a variety of unusual ordered phases [2]. QSLs are novel states of matter of "disordered" nature, which host fractional excitations, such as spinons, and fluctuations of emergent gauge degrees of freedom, such as visons [3, 4]. While it is established that spinons exist in quantum spin chains [5], their counterparts in higher dimensions are much more elusive. Besides the fundamental interest in measuring these exotic states of matter, identifying QSLs in real materials is relevant for topological quantum information processing [6].

While identifying a genuine QSL in a real material should await further investigations, there are multiple reports of magnetically ordered materials with anomalous spin dynamics [7, 8]. A conceivable working hypothesis is that these materials are not far from the "quantum melting point" (QMP) that signals the transition into a QSL phase. The proximity to a QMP implies a potentially strong influence of the nearby QSL phases on the magnetic excitation spectrum [7–12]. For example, magnons are expected to become weakly bound pairs of spinons near the QMP [9, 13]. This phenomenon is clearly beyond the reach of large-S theory because of the fractionalized nature of spinons [8]. These ideas are realized in weakly coupled spin chains [5, 9] and, more recently, in the illuminating context of the Kitaev model [14] and its multiple extensions [15–18]. For instance, recent Raman scattering [19] and inelastic neutron scattering (NS) measurements [20, 21] on α-$RuCl_3$ suggested that this magnetically ordered material hosts fermionic excitations, resembling the Majorana fermions of the Kitaev QSL [14].

Given the abundance of magnetically ordered frustrated magnets which are potentially close to their QMP, it is relevant to look for fingerprints of the nearby liquid state in their magnetic excitation spectrum. A recent report [22] shed light on anomalous observations in an inelastic NS experiment on single crystals of the equilateral triangular-lattice Heisenberg antiferromagnet (TLHAF) $Ba_3CoSb_2O_9$ [23–30]. This quantum magnet comprises triangular layers of Co^{2+} ions carrying effective spin-1/2 magnetic moments. Deviations from a pure 2D Heisenberg model due to anisotropies and 3D couplings are rather small [22, 26] and Dzyaloshinskii-Moriya interactions are essentially precluded because of the highly symmetric crystal structure (space group $P6_3/mmc$). Thus, $Ba_3CoSb_2O_9$ is an almost ideal realization of the quantum TLHAF, a paradigmatic model for frustrated magnets [31].

The ground state of $Ba_3CoSb_2O_9$ is magnetically ordered into the 120° state [32, 33]. However, its spin dynamics still retains various anomalous features [22]. The high frequency ($\gtrsim 2\,\mathrm{meV}$) excitation continuum has a large spectral weight, almost comparable to that of the single-magnon excitations. Furthermore, magnon spectral lines are broadened throughout the entire Brillouin zone. Magnon decays, nonlinear effects in spin-wave (SW) theory stemming from the noncollinear magnetic structure [34–38], are natural contenders to explain these qualitative features in the dynamical structure factor $\mathcal{S}(\mathbf{q},\omega)$. Surprisingly, neither of the anomalous experimental observations can be explained by a conventional $1/S$ expansion [22]. It was found that the small, but non-

negligible, easy-plane anisotropy renders the decay process from one magnon to two-magnon continuum [34–38] ineffective (the kinematic conditions are not satisfied), because one of the two Nambu-Goldstone modes of the isotropic TLHAF is gapped out by the anisotropy. In addition, SW theory significantly overestimates the in-plane magnon bandwidth [22].

Given that impurity effects have been carefully excluded [22], the proximity to a QMP is one possible explanation for the failure of SW theory. In the meantime, the ordered moment of $m_{\rm Q} = 1.53(2)\,\mu_{\rm B}$ [39] is around 79(1)% of the full moment $m_{\rm full} = 1.93\,\mu_{\rm B}$ per Co^{2+} [26], which is rather in close agreement with SW theory applied to this material [22] predicting $m_{\rm Q}/m_{\rm full} = 73\%$. Thus, this ratio is not small enough to conclude the proximity to a QMP [40], while probably not large enough to safely validate the $1/S$ expansion to describe the spin dynamics of the TLHAF. It is hence crucial to validate the spin Hamiltonian of $Ba_3CoSb_2O_9$ in an independent fashion. It is also desired to exclude other extrinsic experimental effects such as magnon-phonon coupling [41].

In this Letter, we demonstrate that the deviations from SW theory observed for $Ba_3CoSb_2O_9$ at zero field [22] are an intrinsic effect induced by quantum fluctuations. To this end, we study the spin dynamics of $Ba_3CoSb_2O_9$ in high magnetic fields. The high fields suppress quantum fluctuations and create favorable conditions for a comparison against SW theory. While SW theory becomes exact for single-magnon excitations above the saturation field $H_{\rm sat}$, it is too high for contemporary NS facilities ($\mu_0 H_{\rm sat} = 31.9$ T for $\mathbf{H} \parallel ab$ and 32.8 T for $\mathbf{H} \parallel c$ [26]). However, it turns out to be sufficient to measure the spin dynamics within the 1/3 magnetization plateau with the up-up-down (UUD) spin structure [24, 26, 28], which extends between $\mu_0 H_{c1} = 9.7$ T and $\mu_0 H_{c2} = 15$ T for $\mathbf{H} \parallel ab$ [29]. In fact, although this phase itself is stabilized by quantum fluctuations [28, 42–44], its gapped spectrum is expected to be well described by SW theory because of the smaller reduction of the ordered moment. Specifically, we will demonstrate that the spectrum within the plateau can be reproduced by the spin Hamiltonian in Ref. 22 with almost identical coupling constants. Our work thus establishes that the anomalous *zero-field* spectrum of $Ba_3CoSb_2O_9$ is intrinsic and most likely caused by the proximity of its magnetic ordering to a QMP. In the meantime, this is the first attempt elucidating the spin dynamics in the quantum UUD phase in the TLHAF material, while such plateau is known to exist also in Cs_2CuBr_4 [45–49].

A single crystal of $Ba_3CoSb_2O_9$ was grown by the floating-zone technique and oriented in the (h, h, l) scattering plane. The neutron diffraction data under magnetic fields applied in the [1,-1,0] direction was obtained by using the CG-4C cold triple-axis spectrometer (CTAX) with the neutron energy fixed at 5.0 meV at High Flux Isotope Reactor (HFIR), Oak Ridge National Laboratory. The magnetic Bragg peaks at (1/3, 1/3, 1) and (1/3, 1/3, 0) were measured at 1.5 K. As depicted in Fig. 1(a), the strong diffraction at both (1/3, 1/3, 1) and (1/3, 1/3, 0) confirms stabilization of the UUD state at $\mu_0 H \geq 9.8$ T, which can be contrasted with the combination of the strong diffraction at (1/3, 1/3, 1) and the lack of intensity at (1/3, 1/3, 0) for the 120° state at $H = 0$.

The dynamical properties of $Ba_3CoSb_2O_9$ in the UUD phase were investigated with the Multi Axis Crystal Spectrometer (MACS) [50] at NIST Center for Neutron Research (NCNR), NIST, and the cold neutron triple-axis spectrometer (V2-FLEXX) [51] at Helmholtz-Zentrum Berlin (HZB). The final energies were fixed at 3.5 meV and 5 meV on the MACS and 3.0 meV on V2-FLEXX. Figures 2(a)–2(c) show the scattering intensity $I(\mathbf{q}, \omega) \equiv k_i/k_f(\mathrm{d}^2\sigma/\mathrm{d}\Omega \mathrm{d}E_f)$ along high-symmetry directions in the reciprocal space at $\mu_0 H = 10.5$ T and $T = 0.5$ K; this temperature is low enough compared to the transition temperature $T_{\rm N} \approx 5$ K to the UUD phase in this field regime [29]. We observed two gapped modes in the in-plane dispersion along with a third one, for which it is not clear whether the gap is nonzero or not due to the limited instrumental resolution [Fig. 2(a)]; if this mode is also gapped, the energy gap should be $\lesssim 0.3$ meV. The dispersion is nearly flat in the out-of-plane direction [Figs. 2(b) and 2(c)].

To compare against the above inelastic NS results in the UUD phase, we consider the same spin Hamiltonian used in Ref. 22 for $\mathbf{H}$ parallel to the a-axis. This is a spin-1/2 XXZ model on the stacked triangular lattice shown in Fig. 1(b), with in-plane nearest-neighbor (NN) exchange J and inter-layer exchange J_c:

$$\mathcal{H} = J \sum_{\langle ij \rangle} \left(S_i^x S_j^x + S_i^y S_j^y + \Delta S_i^z S_j^z \right) + J_c \sum_i \left(S_i^x S_{i+\frac{\hat{c}}{2}}^x + S_i^y S_{i+\frac{\hat{c}}{2}}^y + \Delta S_i^z S_{i+\frac{\hat{c}}{2}}^z \right) - \tilde{H} \sum_i S_i^x, \quad (1)$$

where $\tilde{H} = g_\perp \mu_{\rm B} H$ is the reduced magnetic field and $g_\perp$ is the in-plane component of the g-tensor. $\mathbf{S}_i$ is the effective spin-1/2 operator describing the ground state Kramers doublet of Co^{2+} and $\langle ij \rangle$ denotes the in-plane NN sites. The displacement vector along the c-axis is $\hat{c}/2$ because the unit cell of $Ba_3CoSb_2O_9$ contains two vertically aligned Co^{2+}.

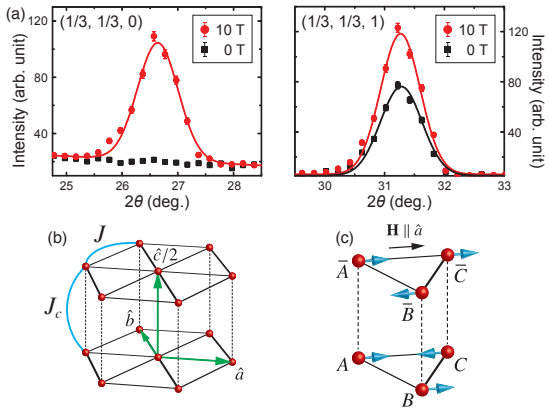

FIG. 1. (a) NS diffraction data at $\mu_0 H = 0$ T and 10 T at $T = 1.5$ K. Error bars in all figures represent one standard deviation. (b) Stacked triangular lattice of Co^{2+} carrying effective spin-1/2 magnetic moments. (c) Spin structure of the UUD state.

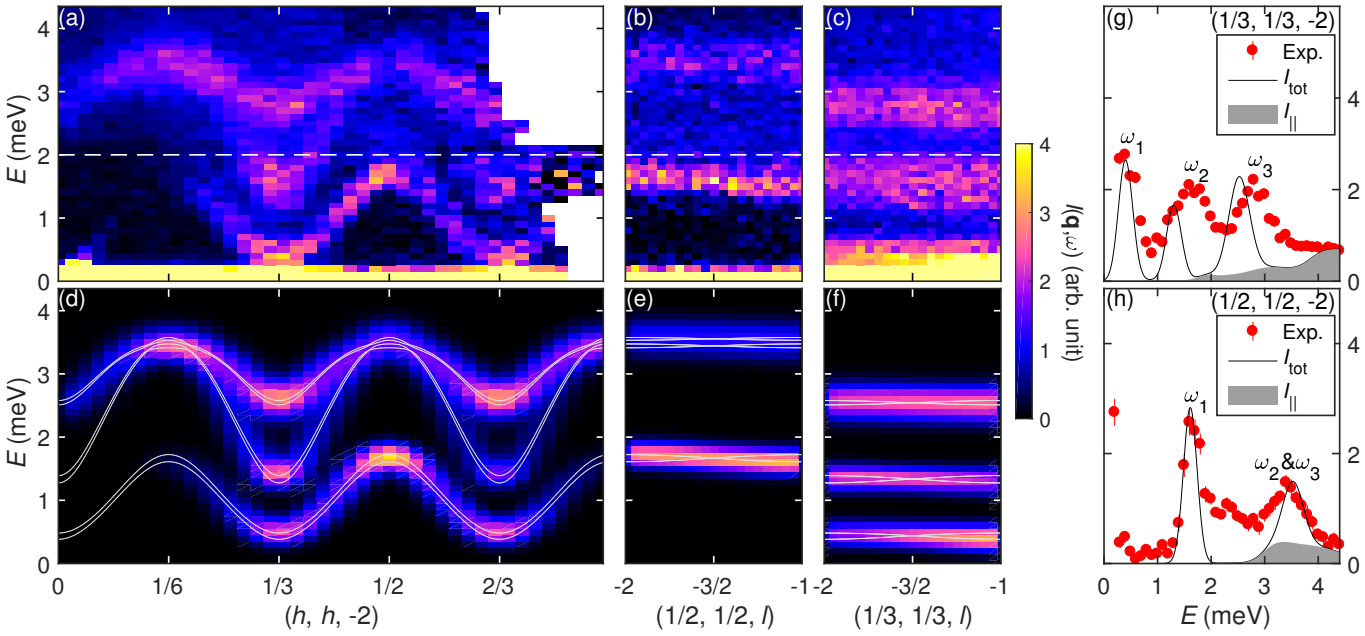

FIG. 2. (a)–(c) Experimental scattering intensity at $\mu_0 H = 10.5\,\mathrm{T}$ and $T = 0.5\,\mathrm{K}$ with momentum transfer (a) in the triangular plane $\mathbf{q} = (h, h, -2)$, and along the c axis with (b) $\mathbf{q} = (1/2, 1/2, l)$ and (c) $\mathbf{q} = (1/3, 1/3, l)$. The energy of the outgoing neutrons is $E_f = 5\,\mathrm{meV}$ (3 meV) above (below) the dashed line. (d)–(f) Calculated transverse part of the scattering intensity, $I_\perp(\mathbf{q}, \omega)$, obtained by the nonlinear SW theory and evaluated along the same momentum cuts as in (a)–(c) for parameters $J = 1.77$ meV, $\Delta = 0.85$, $J_c/J = 0.05$, and $g_\perp = 4.0$. The solid lines show the SW poles. (g) and (h) Energy dependence of the scattering intensity, $I_{\mathrm{tot}}(\mathbf{q}, \omega)$ (solid line), compared to the data for momenta (g) $\mathbf{q} = (1/3, 1/3, -2)$ and (h) $\mathbf{q} = (1/2, 1/2, -2)$. The longitudinal contribution to the scattering intensity, $I_\parallel(\mathbf{q}, \omega)$, is plotted separately as a shaded area.

As first predicted by Chubukov and Golosov for large S [42] and confirmed later on by numerical studies for $S = 1/2$ [43, 44, 52–54], the UUD state is expected to be the ground state of this model (1) for $\Delta \lesssim 1$ and $J_c/J \ll 1$ over a finite window around $\tilde{H} = 3JS$, i.e., 1/3 of the saturation field in the 2D limit ($J_c = 0$). However, in deriving the corresponding SW spectrum, the usual $1/S$ expansion machinery is unapplicable because the UUD state is the classical ground state only on the special line $J_c = 0$, $\tilde{H} = 3JS$, and $\Delta \leq 1$ [55]. Thus, the magnons of the UUD phase derived in the conventional way become unstable away from this line. Fortunately, this instability can be avoided by using a modified approach that was applied to a similar problem for the distorted triangular lattice [56]. The basic idea is that magnon-magnon interactions should enlarge the stability region for the UUD phase around the classical line. To outline our analysis (see Supplemental Material for details [55]), we first expand $\mathcal{H}$ in $1/S$ on the special line by assuming the six-sublattice UUD spin configuration shown in Fig. 1(c). The purpose of this preliminary calculation is to evaluate the leading-order magnon self-energies arising from decoupling the quartic terms in the $1/S$ expansion. In fact, the linear SW Hamiltonian at this stage has two relativistic modes, both of which become gapped after incorporating the self-energy contributions evaluated at $J_c = 0$ and $\tilde{H} = 3JS$ for a given value of $\Delta \leq 1$ [55]. The fully gapped spectrum is robust against a finite $J_c > 0$ and $\tilde{H} \neq 3JS$, implying that the UUD is stable over a finite volume of the phase diagram. The resulting nonlinear SW Hamiltonian, $\mathcal{H}_{\mathrm{NLSW}}$, is the Bogoliubov Hamiltonian for the six-sublattice magnon fields, with the magnon interactions included at the mean-field level. The UUD phase becomes locally unstable when the gap closes.

Figures 2(d)–2(h) show the calculated scattering intensity $I(\mathbf{q}, \omega) \equiv (\gamma r_0/2)^2 |F(\mathbf{q})|^2 \sum_\alpha (1 - \hat{q}^\alpha \hat{q}^\alpha) g_\alpha^2 \mathcal{S}^{\alpha\alpha}(\mathbf{q}, \omega)$ where $F(\mathbf{q})$ denotes the magnetic form factor, $(\gamma r_0/2)^2$ is a constant, $\hat{q}^\alpha = q^\alpha/|\mathbf{q}|$, and $\mathcal{S}^{\alpha\alpha}(\mathbf{q}, \omega)$ are the diagonal components of the dynamical structure factor evaluated at $\mu_0 H = 10.5\,\mathrm{T}$ and $T = 0$. This result is compared against our inelastic NS measurements along different directions of the Brillouin zone in Figs. 2(a)–2(c). Defining the UUD order as along the x axis, transverse spin fluctuations related to single-magnon excitations appear in $\mathcal{S}^{yy}$ and $\mathcal{S}^{zz}$, while longitudinal spin fluctuations corresponding to the two-magnon continuum appear in $\mathcal{S}_\parallel$, denoting the inelastic part of $\mathcal{S}^{xx}$ [55]. Accordingly, the scattering intensity $I(\mathbf{q}, \omega)$ can be separated into transverse $I_\perp$ and longitudinal $I_\parallel$ contributions. To compare with our experiments, the theoretical intensity is convoluted with empirical instrumental energy resolution and momentum binning effects (only the energy resolution is convoluted for $I_\parallel$).

Three bands of scattering associated with six distinct dispersion branches are expected: the lowest band is well isolated, while there is a significant hybridization between the other two around $\mathbf{q} = (1/2, 1/2, l)$ with arbitrary l and related momenta [see Figs. 2(a) and 2(b)]. This implies that

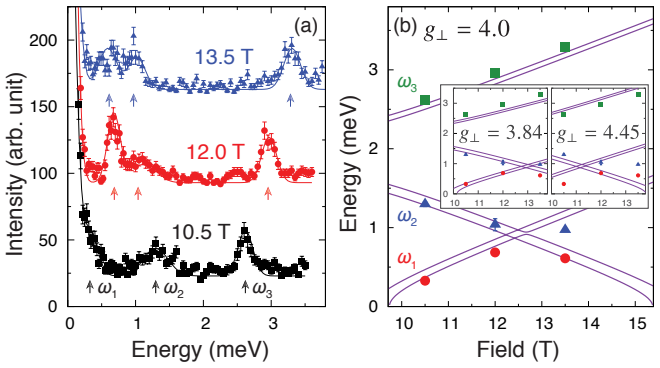

FIG. 3. (a) Constant-q scans at (1/3, 1/3, 1) for the selected values of the magnetic field in the UUD phase at 0.1 K. The solid-lines show the results of the fitting to Gaussian functions. The arrows indicate the SW peaks ω_1–ω_3. (b) Comparison of the fitted SW frequencies ω_1 (circles), ω_2 (triangles), and ω_3 (squares) against the simulation results of poles (lines) based on the nonlinear SW theory for $g_\perp = 4.0$. The inset shows the cases for $g_\perp = 3.84$ [26] and $g_\perp = 4.45$ [30].

$\mu_0 H = 10.5\,\mathrm{T}$ corresponds to $\tilde{H} \lesssim 3JS$ [55]. The best fit with the experiments is obtained for $J = 1.77\,\mathrm{meV}$, $\Delta = 0.85$, and $J_c/J = 0.05$. In addition, we assume $g_\perp = 4.0$, which is slightly larger than $g_\perp = 3.84$ [26] measured with electronic spin resonance (ESR) at $T = 20\,\mathrm{K}$ whereas it is smaller than the recent claim $g_\perp = 4.45$ [30] based on susceptibility measurements [57]. This is to improve the fit to the field dependence of the SW modes, as discussed below. Remarkably, the estimated coupling constants are not very different from those based on the inelastic NS measurements at $H = 0$ probing excitations of the 120° state, $J = 1.7\,\mathrm{meV}$, $\Delta = 0.89$, and $J_c/J = 0.05$ [22]. However, unlike the $H = 0$ case, the agreement between theory and experiment is excellent for the UUD phase. First of all, the calculated bandwidths for the major three bands agree very well with the observed ones, in contrast to the nonlinear SW theory at $H = 0$ which overestimates the overall bandwidth by $\approx 35\%$ [22]. Also, the characteristics of the in-plane dispersion [Fig. 2(d)] and the nearly dispersionless feature in the out-of-plane directions [Figs. 2(e) and 2(f)] are well reproduced. Furthermore, the observed line broadening is reproduced. The broadening arises from the fact that each of the three "bands" actually comprise two poles with comparable amplitudes, which are split by the rather small inter-layer coupling J_c. The corresponding peaks overlap with each other because of the limited energy-momentum resolution. In more details, the linewidths of ω_2 and ω_3 in Figs. 2(g) and 2(h) are slightly broader than the resolution. This broadening can be due to single-to-triple magnon decays [38], which are kinematically allowed.

The lowest-energy branch [Fig. 2(a)] is a massive excitation with a small energy gap $\approx 0.37\,\mathrm{meV}$ at $\mathbf{q} = (1/3, 1/3, 1)$ that can be guessed from the experimental data. The smallness of the gap results from the proximity to the lower quantum critical point at $\mu_0 H_{c1} = 9.7\,\mathrm{T}$ [29], separating the UUD phase from the low-field coplanar phase [28]. In Fig. 3(a), we show the the constant-q scans at (1/3, 1/3, 1) at $\mu_0 H = 10.5$, 12, and 13.5 T in the UUD phase, from which we extract the H-dependence of the SW peaks ω_1–ω_3 of the three major branches, neglecting the splitting due to J_c, which is beyond our instrumental resolution. According to Fig. 3(b), their field dependence agrees well with the nonlinear SW theory. We find that ω_3 increases linearly in H, whereas ω_1 (ω_2) increases (decreases) first, and then decreases (increases), reflecting a level-crossing induced by H.

Thus, the spin excitation spectrum in the UUD phase is very well reproduced by the nonlinear SW calculation. This confirms the validity of the minimal Hamiltonian [Eq. (1)]. SW theory works well for describing the UUD state because the collinear ordering reduces the amplitude of the quantum fluctuations. Indeed, the calculated reduction of the magnetic moment in each sublattice μ, $\delta S_\mu = S - |\langle \mathbf{S}_j \rangle|$ with $j \in \mu$, is very small: $\delta S_A = \delta S_{\bar{A}} = 0.0826$, $\delta S_B = \delta S_{\bar{C}} = 0.0767$, and $\delta S_C = \delta S_{\bar{B}} = 0.145$ for the UUD state illustrated in Fig. 1(c). This is consistent with the very weak intensity of the two-magnon continuum [Figs. 2(g) and 2(h)].

More importantly, the estimated Hamiltonian parameters almost coincide with those in Ref. 22. This observation is particularly important because it confirms the conjecture triggered by the zero-field inelastic NS experiments [22]: the discrepancy between the measured $\mathcal{S}(\mathbf{q}, \omega)$ and the semiclassical theory at $H = 0$ is not rooted in an inadequate spin Hamiltonian. Moreover, it is noteworthy that the UUD state breaks both translational and rotational symmetries of the underlying lattice [see Fig. 1(c)]. Unlike the zero field case, the bonds become inequivalent in the UUD state: two thirds of the in-plane NN spin-pairs are aligned antiferromagnetically, while the other third are ferromagnetically aligned. Hence, the UUD state is more susceptible to magnon-phonon coupling than the zero-field 120° state. The fact that Eq. (1) reproduces the measured excitation spectrum of the UUD state suggests that the magnon-phonon coupling is small in this material and this must hold true down to $H = 0$.

To conclude, our high-field NS experiments mapped the excitations within the 1/3-magnetization plateau of $Ba_3CoSb_2O_9$, a model quantum triangular-lattice Heisenberg antiferromagnet, and confirmed the validity of the spin Hamiltonian considered in Ref. 22. It will be interesting to investigate the applicability range of SW theory in a magnetic field for both $\mathbf{H} \parallel ab$ and $\mathbf{H} \parallel c$ [58]. Our study also excluded magnon-phonon interaction as the possible source for the discrepancy between the zero-field inelastic NS experiments and SW theory, thus calling for a new theoretical approach capable of describing the anomalous spin dynamics of magnetically ordered materials in the proximity of their quantum melting point.

Acknowledgments.— We thank H. Tanaka, A. Chernyshev, and O. Starykh for valuable discussions. We are grateful for the access to the neutron beam time at the neutron facilities at NCNR, BER-2 at Helmholtz-Zentrum Berlin and HFIR operated by ORNL. The research at HFIR at ORNL was sponsored by the Scientific User Facilities Division (T.H., H.B.C.,

and M.M.), Office of Basic Energy Sciences, U.S. DOE. This work utilized MACS supported in part by the National Science Foundation under Agreement No. DMR-1508249. J.M. acknowledges the support of the Ministry of Science and Technology of China (2016YFA0300500). Y.K. acknowledges the financial support by JSPS Grants-in-Aid for Scientific Research under Grant No. JP16H02206. The work at Georgia Tech was supported by ORAU's Ralph E. Powe Junior Faculty Enhancement Award (M.M.). H.D.Z. acknowledges support from NSF-DMR-1350002 and from NHMFL through NSF-DMR-1157490 and the State of Florida.

* yoshitomo.kamiya@riken.jp
† jma3@sjtu.edu.cn

[1] C. Lacroix, P. Mendels, and F. Mila, eds., *Introduction to Frustrated Magnetism: Materials, Experiments, Theory* (Springer-Verlag, Berlin Heidelberg, 2011).
[2] O. A. Starykh, Rep. Prog. Phys. **78**, 052502 (2015).
[3] L. Balents, Nature **464**, 199 (2010).
[4] L. Savary and L. Balents, Rep. Prog. Phys. **80**, 016502 (2017).
[5] M. Mourigal, M. Enderle, A. Klopperpieper, J.-S. Caux, A. Stunault, and H. M. Ronnøw, Nat. Phys **9**, 435 (2013).
[6] C. Nayak, S. H. Simon, A. Stern, M. Freedman, and S. Das Sarma, Rev. Mod. Phys. **80**, 1083 (2008).
[7] R. Coldea, D. A. Tennant, A. M. Tsvelik, and Z. Tylczynski, Phys. Rev. Lett. **86**, 1335 (2001).
[8] B. Dalla Piazza, M. Mourigal, N. B. Christensen, G. J. Nilsen, P. Tregenna-Piggott, T. G. Perring, M. Enderle, D. F. McMorrow, D. A. Ivanov, and H. M. Ronnøw, Nat. Phys **11**, 62 (2015).
[9] M. Kohno, O. A. Starykh, and L. Balents, Nat. Phys **3**, 790 (2007).
[10] Y. Kamiya, Y. Kato, J. Nasu, and Y. Motome, Phys. Rev. B **92**, 100403 (2015).
[11] X.-Y. Song, Y.-Z. You, and L. Balents, Phys. Rev. Lett. **117**, 037209 (2016).
[12] M. Gohlke, R. Verresen, R. Moessner, and F. Pollmann, arXiv: 1701.04678 (unpublished).
[13] A. V. Chubukov and O. A. Starykh, Phys. Rev. B **52**, 440 (1995).
[14] A. Kitaev, Ann. Phys. (N.Y.) **321**, 2 (2006).
[15] G. Jackeli and G. Khaliullin, Phys. Rev. Lett. **102**, 017205 (2009).
[16] J. Chaloupka, G. Jackeli, and G. Khaliullin, Phys. Rev. Lett. **110**, 097204 (2013).
[17] J. G. Rau, E. K.-H. Lee, and H.-Y. Kee, Phys. Rev. Lett. **112**, 077204 (2014).
[18] J. Nasu, Y. Kato, J. Yoshitake, Y. Kamiya, and Y. Motome, arXiv: 1610.07343 (unpublished).
[19] J. Nasu, J. Knolle, D. L. Kovrizhin, Y. Motome, and R. Moessner, Nat. Phys. **12**, 912 (2016).
[20] A. Banerjee, C. A. Bridges, J. Q. Yan, A. A. Aczel, L. Li, M. B. Stone, G. E. Granroth, M. D. Lumsden, Y. Yiu, J. Knolle, S. Bhattacharjee, D. L. Kovrizhin, R. Moessner, D. A. Tennant, D. G. Mandrus, and S. E. Nagler, Nat. Mater. **15**, 733 (2016).
[21] A. Banerjee, J. Yan, J. Knolle, C. A. Bridges, M. B. Stone, M. D. Lumsden, D. G. Mandrus, D. A. Tennant, R. Moessner, and S. Nagler, arXiv: 1609.00103 (unpublished).
[22] J. Ma, Y. Kamiya, T. Hong, H. B. Cao, G. Ehlers, W. Tian, C. D. Batista, Z. L. Dun, H. D. Zhou, and M. Matsuda, Phys. Rev. Lett. **116**, 087201 (2016).
[23] Y. Doi, Y. Hinatsu, and K. Ohoyama, J. Phys.: Condens. Matter **16**, 8923 (2004).
[24] Y. Shirata, H. Tanaka, A. Matsuo, and K. Kindo, Phys. Rev. Lett. **108**, 057205 (2012).
[25] H. D. Zhou, C. Xu, A. M. Hallas, H. J. Silverstein, C. R. Wiebe, I. Umegaki, J. Q. Yan, T. P. Murphy, J.-H. Park, Y. Qiu, J. R. D. Copley, J. S. Gardner, and Y. Takano, Phys. Rev. Lett. **109**, 267206 (2012).
[26] T. Susuki, N. Kurita, T. Tanaka, H. Nojiri, A. Matsuo, K. Kindo, and H. Tanaka, Phys. Rev. Lett. **110**, 267201 (2013).
[27] K. Naruse, T. Kawamata, M. Ohno, Y. Matsuoka, H. Sudo, H. Nagasawa, Y. Hagiya, T. Sasaki, and Y. Koike, J. Phys.: Conf. Series **568**, 042014 (2014).
[28] G. Koutroulakis, T. Zhou, Y. Kamiya, J. D. Thompson, H. D. Zhou, C. D. Batista, and S. E. Brown, Phys. Rev. B **91**, 024410 (2015).
[29] G. Quirion, M. Lapointe-Major, M. Poirier, J. A. Quilliam, Z. L. Dun, and H. D. Zhou, Phys. Rev. B **92**, 014414 (2015).
[30] A. Sera, Y. Kousaka, J. Akimitsu, M. Sera, T. Kawamata, Y. Koike, and K. Inoue, Phys. Rev. B **94**, 214408 (2016).
[31] P. Anderson, Mater. Res. Bull. **8**, 153 (1973).
[32] L. Capriotti, A. E. Trumper, and S. Sorella, Phys. Rev. Lett. **82**, 3899 (1999).
[33] S. R. White and A. L. Chernyshev, Phys. Rev. Lett. **99**, 127004 (2007).
[34] A. L. Chernyshev and M. E. Zhitomirsky, Phys. Rev. Lett. **97**, 207202 (2006).
[35] O. A. Starykh, A. V. Chubukov, and A. G. Abanov, Phys. Rev. B **74**, 180403 (2006).
[36] A. L. Chernyshev and M. E. Zhitomirsky, Phys. Rev. B **79**, 144416 (2009).
[37] M. Mourigal, W. T. Fuhrman, A. L. Chernyshev, and M. E. Zhitomirsky, Phys. Rev. B **88**, 094407 (2013).
[38] M. E. Zhitomirsky and A. L. Chernyshev, Rev. Mod. Phys. **85**, 219 (2013).
[39] The ordered moment is estimated from the NS diffraction data presented in Ref. 22. Here, the magnetic form factor is corrected with the orbital contribution.
[40] We also note that the ordered moment per se is not a very sensitive measure of the proximity to a QMP, as it can change rather rapidly near a QMP.
[41] K. Park, J. Oh, J. C. Leiner, J. Jeong, K. C. Rule, M. D. Le, and J.-G. Park, Phys. Rev. B **94**, 104421 (2016).
[42] A. V. Chubukov and D. I. Golosov, J. Phys.: Condens. Matter **3**, 69 (1991).
[43] D. Yamamoto, G. Marmorini, and I. Danshita, Phys. Rev. Lett. **112**, 127203 (2014).
[44] D. Yamamoto, G. Marmorini, and I. Danshita, Phys. Rev. Lett. **114**, 027201 (2015).
[45] T. Ono, H. Tanaka, H. Aruga Katori, F. Ishikawa, H. Mitamura, and T. Goto, Phys. Rev. B **67**, 104431 (2003).
[46] T. Ono, H. Tanaka, O. Kolomiyets, H. Mitamura, T. Goto, K. Nakajima, A. Oosawa, Y. Koike, K. Kakurai, J. Klenke, P. Smeibidle, and M. Meiner, J. Phys.: Condens. Matter **16**, S773 (2004).
[47] T. Ono, H. Tanaka, O. Kolomiyets, H. Mitamura, F. Ishikawa, T. Goto, K. Nakajima, A. Oosawa, Y. Koike, K. Kakurai, J. Klenke, P. Smeibidle, M. Meiner, R. Coldea, A. D. Tennant, and J. Ollivier, Prog. Theor. Phys. Suppl. **159**, 217 (2005).
[48] H. Tsujii, C. R. Rotundu, T. Ono, H. Tanaka, B. Andraka, K. Ingersent, and Y. Takano, Phys. Rev. B **76**, 060406 (2007).
[49] N. A. Fortune, S. T. Hannahs, Y. Yoshida, T. E. Sherline, T. Ono, H. Tanaka, and Y. Takano, Phys. Rev. Lett. **102**, 257201

(2009).
[50] J. A. Rodriguez, D. M. Adler, P. C. Brand, C. Broholm, J. C. Cook, C. Brocker, R. Hammond, Z. Huang, P. Hundertmark, J. W. Lynn, N. C. Maliszewskyj, J. Moyer, J. Orndorff, D. Pierce, T. D. Pike, G. Scharfstein, S. A. Smee, and R. Vilaseca, Meas. Sci. Technol. **19**, 034023 (2008).
[51] M. Le, D. Quintero-Castro, R. Toft-Petersen, F. Groitl, M. Skoulatos, K. Rule, and K. Habicht, Nucl. Instrum. Methods Phys. Res. Sect. A **729**, 220 (2013).
[52] D. J. J. Farnell, R. Zinke, J. Schulenburg, and J. Richter, J. Phys.: Condens. Matter **21**, 406002 (2009).
[53] T. Sakai and H. Nakano, Phys. Rev. B **83**, 100405 (2011).
[54] R. Chen, H. Ju, H.-C. Jiang, O. A. Starykh, and L. Balents, Phys. Rev. B **87**, 165123 (2013).
[55] See Supplemental Material.
[56] J. Alicea, A. V. Chubukov, and O. A. Starykh, Phys. Rev. Lett. **102**, 137201 (2009).
[57] The discrepancy about $g_\perp$ has to be resolved with either high-field magnetization or ESR measurements at $T \gg J$ to exclude effects of short-range spin correlations.
[58] P. A. Maksimov, M. E. Zhitomirsky, and A. L. Chernyshev, Phys. Rev. B **94**, 140407 (2016).

—

Supplemental Material

I. CLASSICAL GROUND STATE

The UUD state [Fig. S1(a)] is not the classical ground state of the easy-plane *XXZ* model on the stacked triangular-lattice in a magnetic field applied along the *a*-axis. To show this, we take the classical version of the Hamiltonian defined in Eq. (1) in the main text, and assume that every spin is lying in the *ab* plane, as favored by the anisotropy and the external field [28]. By introducing the unit length classical spin $\mathbf{\Omega}_j = (\Omega_j^x, \Omega_j^y, \Omega_j^z)$ at each site j, the classical Hamiltonian apart from irrelevant constant terms can be written as

$$\mathcal{H}_{\text{classical}} = \frac{1}{2} JS^2 \sum_{\triangle} \left(\mathbf{\Omega}_{\triangle,1} + \mathbf{\Omega}_{\triangle,2} + \mathbf{\Omega}_{\triangle,3} - \frac{\tilde{\mathbf{H}}}{3JS} \right)^2 + J_c S^2 \sum_i \left(\Omega_i^x \Omega_{i+\hat{c}/2}^x + \Omega_i^y \Omega_{i+\hat{c}/2}^y \right), \tag{S1}$$

under the assumption of $\Omega_j^z = 0$, $\forall j$, where $\tilde{\mathbf{H}} = g_\perp \mu_B \mathbf{H}$ is in the *ab* plane. The summation of $\sum_\triangle$ means that we have divided the in-plane bonds in each triangular lattice layer into upward triangles ($\triangle$) and $j = (\triangle, 1)$, $(\triangle, 2)$, and $(\triangle, 3)$ are the three sites on each triangle (a given site is shared by three neighboring upward triangles, but this does not cause any complication in the following analysis). For $J_c = 0$, any spin configuration satisfying

$$\mathbf{\Omega}_{\triangle,1} + \mathbf{\Omega}_{\triangle,2} + \mathbf{\Omega}_{\triangle,3} = \frac{\tilde{\mathbf{H}}}{3JS}, \quad \forall \triangle, \tag{S2}$$

is a classical ground state. In particular, at $\tilde{H} = 3JS$, the classical ground state manifold includes the UUD state. To show that the UUD state is not the classical ground state for $J_c > 0$, we work in the subspace with fixed $M^x = N_{\text{spin}}^{-1} \sum_j \Omega_j^x = 1/3$ (N_{spin} is the total number of spins) and consider a one-parameter deformation of the spin configuration parametrized by $0 \le \theta \le \pi$, as illustrated in Fig. S1(b). As this transformation does not change $M_x = 1/3$, the first term in Eq. (S1) does not change under this transformation. On the other hand, we find that the classical energy for the inter-layer coupling changes as

$$E_c(\theta) = 2J_c S^2 (\cos 2\theta - 2\cos\theta) \tag{S3}$$

per magnetic unit cell, which is minimized at $\theta = \pi/3$ for $J_c > 0$ instead of the $\theta = 0$ value corresponding to the UUD state. Since the UUD state has $M^x = 1/3$ for $\mathbf{H} \parallel \hat{a}$, this analysis shows that it is not the classical ground state for $J_c > 0$.

II. SPIN WAVE THEORY FOR THE UP-UP-DOWN PHASE IN THE QUASI-2D SYSTEM

A. Nonlinear spin wave Hamiltonian

As mentioned in the main text, it is expected that magnon-magnon interactions can stabilize the UUD state, in spite of the fact that it is not a ground state of $\mathcal{H}_{\text{classical}}$. The physical reasoning behind this statement is that the UUD state is the ground state of the antiferromagnetic triangular Heisenberg model over a *finite window* of magnetic field value. Given the gapped nature of the excitation spectrum, it is expected that this phase should extend up to a nonzero value of J_c (quasi-2D system).

To derive the corresponding SW spectrum, we first work on the 2D limit, $J_c = 0$, for a given value of $\Delta \le 1$ exactly at $\tilde{H} = 3JS$, which are the conditions for the UUD state to be the classical ground state. The purpose of our analysis at this stage is to derive the quadratic Hamiltonian with which we evaluate mean-field (MF) parameters. We apply the local transformation,

$$S_j^x = \tilde{S}_j^z, \quad S_j^y = \tilde{S}_j^y, \quad S_j^z = -\tilde{S}_j^x, \tag{S4}$$

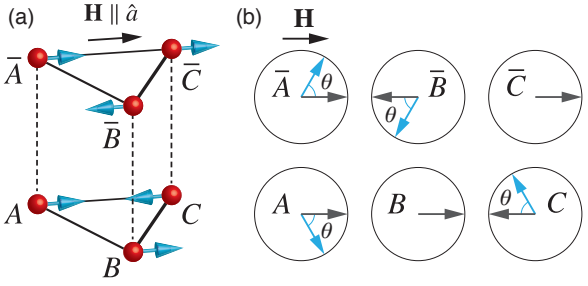

FIG. S1. (a) Spin configuration of the UUD state. (b) One-parameter deformation of the UUD state. The spins of sublattices B and $\bar{C}$ are fixed.

for the sublattices with up-spins (namely, A, B, $\bar{A}$, and $\bar{C}$) and

$$S^x_j = -\tilde{S}^z_j, \quad S^y_j = \tilde{S}^y_j, \quad S^z_j = \tilde{S}^x_j, \tag{S5}$$

for those with down-spins (C and $\bar{B}$) by assuming the UUD state shown in Fig. S1(a). The Holstein-Primakoff bosons are defined relative to the polarized state of $\tilde{\mathbf{S}}_j$:

$$\begin{aligned}
\tilde{S}^z_j &= S - a^\dagger_{\mu,j} a_{\mu,j}, \\
\tilde{S}^+_j &= \tilde{S}^x_j + i\tilde{S}^y_j \approx \sqrt{2S}\left(1 - \frac{a^\dagger_{\mu,j} a_{\mu,j}}{4S}\right) a_{\mu,j}, \\
\tilde{S}^-_j &= \left(\tilde{S}^+_j\right)^\dagger,
\end{aligned} \tag{S6}$$

for each sublattice $1 \le \mu \le 6$ corresponding to A, B, C, $\bar{A}$, $\bar{B}$, and $\bar{C}$ in this order. We have truncated the expansion the square roots in the transformation at the order relevant for deriving the quartic term. By the Fourier transformation, $a_{\mu,\mathbf{k}} = (1/N_{\text{u.c.}})^{1/2} \sum_{j\in\mu} e^{-i\mathbf{k}\cdot\mathbf{r}_j} a_{\mu,j}$ with $N_{\text{u.c.}} = N_{\text{spin}}/6$, the quadratic part of the SW Hamiltonian is given by

$$\mathcal{H}^0_{\text{LSW}} = \mathcal{H}^0_{\text{LSW,even}} + \mathcal{H}^0_{\text{LSW,odd}}, \tag{S7}$$

where the constant term has been dropped and

$$\mathcal{H}^0_{\text{LSW,even}} = \frac{S}{2} \sum_{\mathbf{k}\in\text{RBZ}} \begin{pmatrix} (\mathbf{a}^\dagger_{\mathbf{k}})^{\text{T}} & (\mathbf{a}_{-\mathbf{k}})^{\text{T}} \end{pmatrix} \begin{pmatrix} H^0_{11,\mathbf{k}} & H^0_{12,\mathbf{k}} \\ H^0_{21,\mathbf{k}} & H^0_{22,\mathbf{k}} \end{pmatrix} \begin{pmatrix} \mathbf{a}_{\mathbf{k}} \\ \mathbf{a}^\dagger_{-\mathbf{k}} \end{pmatrix}, \tag{S8}$$

with

$$\mathbf{a}_{\mathbf{k}} = \begin{pmatrix} a_{A,\mathbf{k}} \\ a_{B,\mathbf{k}} \\ a_{C,\mathbf{k}} \end{pmatrix} \equiv \begin{pmatrix} a_{1,\mathbf{k}} \\ a_{2,\mathbf{k}} \\ a_{3,\mathbf{k}} \end{pmatrix}, \quad \mathbf{a}^\dagger_{-\mathbf{k}} = \begin{pmatrix} a^\dagger_{A,-\mathbf{k}} \\ a^\dagger_{B,-\mathbf{k}} \\ a^\dagger_{C,-\mathbf{k}} \end{pmatrix} \equiv \begin{pmatrix} a^\dagger_{1,-\mathbf{k}} \\ a^\dagger_{2,-\mathbf{k}} \\ a^\dagger_{3,-\mathbf{k}} \end{pmatrix}, \tag{S9}$$

is the contribution from the even layers (sublattices A–C). Here, $H^0_{11,\mathbf{k}} = H^0_{22,\mathbf{k}}$, $H^0_{12,\mathbf{k}} = H^0_{21,\mathbf{k}}$, and

$$\begin{aligned}
H^0_{11,\mathbf{k}} &= \begin{pmatrix} S^{-1}\tilde{H} & \frac{3}{2}J(1+\Delta)\gamma_{\mathbf{k}} & \frac{3}{2}J(1-\Delta)\gamma_{-\mathbf{k}} \\ \frac{3}{2}J(1+\Delta)\gamma_{-\mathbf{k}} & S^{-1}\tilde{H} & \frac{3}{2}J(1-\Delta)\gamma_{\mathbf{k}} \\ \frac{3}{2}J(1-\Delta)\gamma_{\mathbf{k}} & \frac{3}{2}J(1-\Delta)\gamma_{-\mathbf{k}} & 6J - S^{-1}\tilde{H} \end{pmatrix}, \\
H^0_{12,\mathbf{k}} &= \begin{pmatrix} 0 & -\frac{3}{2}J(1-\Delta)\gamma_{\mathbf{k}} & -\frac{3}{2}J(1+\Delta)\gamma_{-\mathbf{k}} \\ -\frac{3}{2}J(1-\Delta)\gamma_{-\mathbf{k}} & 0 & -\frac{3}{2}J(1+\Delta)\gamma_{\mathbf{k}} \\ -\frac{3}{2}J(1+\Delta)\gamma_{\mathbf{k}} & -\frac{3}{2}J(1+\Delta)\gamma_{-\mathbf{k}} & 0 \end{pmatrix},
\end{aligned} \tag{S10}$$

where $\gamma_{\mathbf{k}} = \frac{1}{3}(e^{i\mathbf{k}\cdot\mathbf{a}} + e^{i\mathbf{k}\cdot\mathbf{b}} + e^{-i\mathbf{k}\cdot(\mathbf{a}+\mathbf{b})})$. The summation over $\mathbf{k}$ in Eq. (S8) is confined to the reduced Brillouin zone (RBZ) corresponding to the magnetic unit cell of the UUD state (below, this type of summations will be simply denoted as $\sum_{\mathbf{k}}$). Also, the contribution from the odd layers (sublattices $\bar{A}$–$\bar{C}$) is

$$\mathcal{H}^0_{\text{LSW,odd}} = \frac{S}{2} \sum_{\mathbf{k}} \begin{pmatrix} (\bar{\mathbf{a}}^\dagger_{\mathbf{k}})^{\text{T}} & (\bar{\mathbf{a}}_{-\mathbf{k}})^{\text{T}} \end{pmatrix} \begin{pmatrix} \bar{H}^0_{11,\mathbf{k}} & \bar{H}^0_{12,\mathbf{k}} \\ \bar{H}^0_{21,\mathbf{k}} & \bar{H}^0_{22,\mathbf{k}} \end{pmatrix} \begin{pmatrix} \bar{\mathbf{a}}_{\mathbf{k}} \\ \bar{\mathbf{a}}^\dagger_{-\mathbf{k}} \end{pmatrix}, \tag{S11}$$

with

$$\bar{\mathbf{a}}_{\mathbf{k}} = \begin{pmatrix} a_{\bar{A},\mathbf{k}} \\ a_{\bar{B},\mathbf{k}} \\ a_{\bar{C},\mathbf{k}} \end{pmatrix} \equiv \begin{pmatrix} a_{4,\mathbf{k}} \\ a_{5,\mathbf{k}} \\ a_{6,\mathbf{k}} \end{pmatrix}, \quad \bar{\mathbf{a}}^\dagger_{-\mathbf{k}} = \begin{pmatrix} a^\dagger_{\bar{A},-\mathbf{k}} \\ a^\dagger_{\bar{B},-\mathbf{k}} \\ a^\dagger_{\bar{C},-\mathbf{k}} \end{pmatrix} \equiv \begin{pmatrix} a^\dagger_{4,-\mathbf{k}} \\ a^\dagger_{5,-\mathbf{k}} \\ a^\dagger_{6,-\mathbf{k}} \end{pmatrix}, \tag{S12}$$

and the coefficient matrices can be related to those for the even layers simply by permuting indices:

$$\begin{aligned}
\bar{H}^0_{11,\mathbf{k}} = \bar{H}^0_{22,\mathbf{k}} &= \begin{pmatrix} 0 & 1 & 0 \\ 0 & 0 & 1 \\ 1 & 0 & 0 \end{pmatrix} H^0_{11,\mathbf{k}} \begin{pmatrix} 0 & 0 & 1 \\ 1 & 0 & 0 \\ 0 & 1 & 0 \end{pmatrix}, \\
\bar{H}^0_{12,\mathbf{k}} = \bar{H}^0_{21,\mathbf{k}} &= \begin{pmatrix} 0 & 1 & 0 \\ 0 & 0 & 1 \\ 1 & 0 & 0 \end{pmatrix} H^0_{12,\mathbf{k}} \begin{pmatrix} 0 & 0 & 1 \\ 1 & 0 & 0 \\ 0 & 1 & 0 \end{pmatrix}.
\end{aligned} \tag{S13}$$

Under the special condition of $J_c = 0$, $\tilde{H} = 3JS$, and $\Delta < 1$, the quadratic Hamiltonian in Eq. (S7) is positive semi-definite. Hence we can define the following MF parameters symmetrized by using translational and rotational invariance:

$$\begin{aligned}
\rho_\mu &= \frac{1}{N_{\text{u.c.}}} \sum_{j\in\mu} \langle a^\dagger_{\mu,j} a_{\mu,j} \rangle_0, \\
\delta_\mu &= \frac{1}{N_{\text{u.c.}}} \sum_{j\in\mu} \langle (a_{\mu,j})^2 \rangle_0, \\
\xi_{\mu\nu} &= \frac{1}{3N_{\text{u.c.}}} \sum_{j\in\mu} \sum_{\hat{\eta}_{\mu\nu}} \langle a^\dagger_{\mu,j} a_{\nu,j+\hat{\eta}_{\mu\nu}} \rangle_0, \\
\zeta_{\mu\nu} &= \frac{1}{3N_{\text{u.c.}}} \sum_{j\in\mu} \sum_{\hat{\eta}_{\mu\nu}} \langle a_{\mu,j} a_{\nu,j+\hat{\eta}_{\mu\nu}} \rangle_0,
\end{aligned} \tag{S14}$$

where $\hat{\eta}_{\mu\nu}$ represents the in-plane displacement vector for site $j \in \mu$ to reach a NN site in sublattice ν. The mean values $\langle ... \rangle_0$ are evaluated with the ground state of $\mathcal{H}^0_{\text{LSW}}$. We note that the MF parameters for odd (even) layers can be obtained simply from those for even (odd) layers as

$$\begin{aligned}
&\rho_{\bar{A}} = \rho_B, \quad \rho_{\bar{B}} = \rho_C, \quad \rho_{\bar{C}} = \rho_A, \\
&\delta_{\bar{A}} = \delta_B, \quad \delta_{\bar{B}} = \delta_C, \quad \delta_{\bar{C}} = \delta_A, \\
&\xi_{\bar{A}\bar{B}} = \xi_{BC}, \quad \xi_{\bar{B}\bar{C}} = \xi_{CA}, \quad \xi_{\bar{C}\bar{A}} = \xi_{AB}, \\
&\zeta_{\bar{A}\bar{B}} = \zeta_{BC}, \quad \zeta_{\bar{B}\bar{C}} = \zeta_{CA}, \quad \zeta_{\bar{C}\bar{A}} = \zeta_{AB}.
\end{aligned} \tag{S15}$$

The excitation spectrum of $\mathcal{H}^0_{\text{LSW}}$ retains two relativistic modes at $\mathbf{k} = 0$ [Fig. S2(a)]. To turn on the deviations from the condition of $J_c = 0$ and $\tilde{H} = 3JS$, we include nonlinear terms, which indeed will gap out these modes [Fig. S2(b)]. At this stage, the nonlinear terms correspond to the decoupling of the intra-layer quartic terms. The inter-layer coupling will also be included later on, where both the linear SW term and the decoupling of the quartic terms will be added to our nonlinear SW Hamiltonian $\mathcal{H}_{\text{NLSW}}$. By combining all the contributions, we obtain,

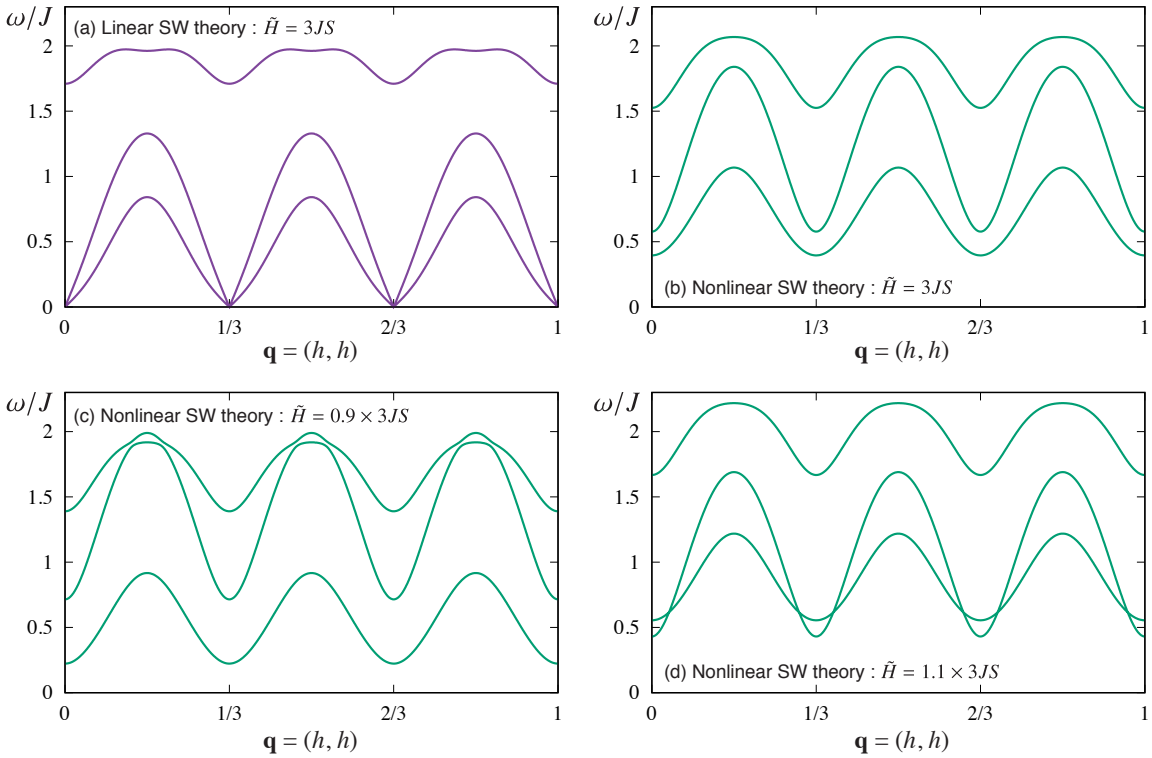
(a) Linear SW theory : $\tilde{H} = 3JS$
(b) Nonlinear SW theory : $\tilde{H} = 3JS$
(c) Nonlinear SW theory : $\tilde{H} = 0.9 \times 3JS$
(d) Nonlinear SW theory : $\tilde{H} = 1.1 \times 3JS$
ω/J
$\mathbf{q} = (h, h)$

FIG. S2. (a) Magnon frequencies in the linear SW approximation at $\tilde{H} = 3JS$ with two gapless modes at $\mathbf{q} = (0,0)$, (1/3,1/3), and (2/3, 2/3). Magnon frequencies in the nonlinear SW approximation at (b) $\tilde{H} = 3JS$, (c) $\tilde{H} = 0.9 \times 3JS$, and (d) $\tilde{H} = 1.1 \times 3JS$. All the results are for $J_c = 0$ and $\Delta = 0.85$. The condition of $J_c \neq 0$ leads to the splitting of these three branches into six.

$$\mathcal{H}_{\mathrm{NLSW}} = \frac{S}{2}\sum_{\mathbf{k}}\left((\mathbf{a}_{\mathbf{k}}^{\dagger})^{\mathrm{T}}\ (\bar{\mathbf{a}}_{\mathbf{k}}^{\dagger})^{\mathrm{T}}\ (\mathbf{a}_{-\mathbf{k}})^{\mathrm{T}}\ (\bar{\mathbf{a}}_{-\mathbf{k}})^{\mathrm{T}}\right)\begin{pmatrix} H_{\mathrm{ee},\mathbf{k}} & H_{\mathrm{eo},\mathbf{k}} & H'_{\mathrm{ee},\mathbf{k}} & H'_{\mathrm{eo},\mathbf{k}} \\ (H_{\mathrm{eo},\mathbf{k}})^{\dagger} & H_{\mathrm{oo},\mathbf{k}} & (H'_{\mathrm{eo},-\mathbf{k}})^{\mathrm{T}} & H'_{\mathrm{oo},\mathbf{k}} \\ (H'_{\mathrm{ee},-\mathbf{k}})^{*} & (H'_{\mathrm{eo},-\mathbf{k}})^{*} & (H_{\mathrm{ee},-\mathbf{k}})^{*} & (H_{\mathrm{eo},-\mathbf{k}})^{*} \\ (H'_{\mathrm{eo},\mathbf{k}})^{\dagger} & (H'_{\mathrm{oo},-\mathbf{k}})^{*} & (H_{\mathrm{eo},-\mathbf{k}})^{\mathrm{T}} & (H_{\mathrm{oo},-\mathbf{k}})^{*} \end{pmatrix}\begin{pmatrix} \mathbf{a}_{\mathbf{k}} \\ \bar{\mathbf{a}}_{\mathbf{k}} \\ \mathbf{a}_{-\mathbf{k}}^{\dagger} \\ \bar{\mathbf{a}}_{-\mathbf{k}}^{\dagger} \end{pmatrix}, \tag{S16}$$

with

$$H_{\mathrm{ee},\mathbf{k}} = H^{0}_{11,\mathbf{k}} + \begin{pmatrix} -2J_c & 0 & 0 \\ 0 & 2J_c & 0 \\ 0 & 0 & 2J_c \end{pmatrix} + S^{-1}\begin{pmatrix} \mu^{A}_{\mathrm{MF}} & \left(t^{AB}_{\mathrm{MF}}\right)^{*}\gamma_{\mathbf{k}} & t^{CA}_{\mathrm{MF}}\gamma_{-\mathbf{k}} \\ t^{AB}_{\mathrm{MF}}\gamma_{-\mathbf{k}} & \mu^{B}_{\mathrm{MF}} & \left(t^{BC}_{\mathrm{MF}}\right)^{*}\gamma_{\mathbf{k}} \\ \left(t^{CA}_{\mathrm{MF}}\right)^{*}\gamma_{\mathbf{k}} & t^{BC}_{\mathrm{MF}}\gamma_{-\mathbf{k}} & \mu^{C}_{\mathrm{MF}} \end{pmatrix} + S^{-1}\begin{pmatrix} 2J_c\rho_{\bar{A}} & 0 & 0 \\ 0 & -2J_c\rho_{\bar{B}} & 0 \\ 0 & 0 & -2J_c\rho_{\bar{C}} \end{pmatrix},$$

$$H_{\mathrm{oo},\mathbf{k}} = \bar{H}^{0}_{11,\mathbf{k}} + \begin{pmatrix} -2J_c & 0 & 0 \\ 0 & 2J_c & 0 \\ 0 & 0 & 2J_c \end{pmatrix} + S^{-1}\begin{pmatrix} \mu^{\bar{A}}_{\mathrm{MF}} & \left(t^{\bar{A}\bar{B}}_{\mathrm{MF}}\right)^{*}\gamma_{\mathbf{k}} & t^{\bar{C}\bar{A}}_{\mathrm{MF}}\gamma_{-\mathbf{k}} \\ t^{\bar{A}\bar{B}}_{\mathrm{MF}}\gamma_{-\mathbf{k}} & \mu^{\bar{B}}_{\mathrm{MF}} & \left(t^{\bar{B}\bar{C}}_{\mathrm{MF}}\right)^{*}\gamma_{\mathbf{k}} \\ \left(t^{\bar{C}\bar{A}}_{\mathrm{MF}}\right)^{*}\gamma_{\mathbf{k}} & t^{\bar{B}\bar{C}}_{\mathrm{MF}}\gamma_{-\mathbf{k}} & \mu^{\bar{C}}_{\mathrm{MF}} \end{pmatrix} + S^{-1}\begin{pmatrix} 2J_c\rho_{A} & 0 & 0 \\ 0 & -2J_c\rho_{B} & 0 \\ 0 & 0 & -2J_c\rho_{C} \end{pmatrix},$$

$$H'_{\mathrm{ee},\mathbf{k}} = H^{0}_{12,\mathbf{k}} + S^{-1}\begin{pmatrix} \Gamma^{A}_{\mathrm{MF}} & g^{AB}_{\mathrm{MF}}\gamma_{\mathbf{k}} & g^{CA}_{\mathrm{MF}}\gamma_{-\mathbf{k}} \\ g^{AB}_{\mathrm{MF}}\gamma_{-\mathbf{k}} & \Gamma^{B}_{\mathrm{MF}} & g^{BC}_{\mathrm{MF}}\gamma_{\mathbf{k}} \\ g^{CA}_{\mathrm{MF}}\gamma_{\mathbf{k}} & g^{BC}_{\mathrm{MF}}\gamma_{-\mathbf{k}} & \Gamma^{C}_{\mathrm{MF}} \end{pmatrix}, \quad H'_{\mathrm{oo},\mathbf{k}} = \bar{H}^{0}_{12,\mathbf{k}} + S^{-1}\begin{pmatrix} \Gamma^{\bar{A}}_{\mathrm{MF}} & g^{\bar{A}\bar{B}}_{\mathrm{MF}}\gamma_{\mathbf{k}} & g^{\bar{C}\bar{A}}_{\mathrm{MF}}\gamma_{-\mathbf{k}} \\ g^{\bar{A}\bar{B}}_{\mathrm{MF}}\gamma_{-\mathbf{k}} & \Gamma^{\bar{B}}_{\mathrm{MF}} & g^{\bar{B}\bar{C}}_{\mathrm{MF}}\gamma_{\mathbf{k}} \\ g^{\bar{C}\bar{A}}_{\mathrm{MF}}\gamma_{\mathbf{k}} & g^{\bar{B}\bar{C}}_{\mathrm{MF}}\gamma_{-\mathbf{k}} & \Gamma^{\bar{C}}_{\mathrm{MF}} \end{pmatrix},$$

$$H_{\mathrm{eo},\mathbf{k}} = \cos k_3\begin{pmatrix} J_c(1+\Delta) & 0 & 0 \\ 0 & J_c(1-\Delta) & 0 \\ 0 & 0 & J_c(1-\Delta) \end{pmatrix} + S^{-1}\cos k_3\begin{pmatrix} \left(t^{A\bar{A}}_{\mathrm{MF}}\right)^{*} & 0 & 0 \\ 0 & \left(t^{B\bar{B}}_{\mathrm{MF}}\right)^{*} & 0 \\ 0 & 0 & \left(t^{C\bar{C}}_{\mathrm{MF}}\right)^{*} \end{pmatrix},$$

$$H'_{\mathrm{eo},\mathbf{k}} = \cos k_3 \begin{pmatrix} -J_c(1-\Delta) & 0 & 0 \\ 0 & -J_c(1+\Delta) & 0 \\ 0 & 0 & -J_c(1+\Delta) \end{pmatrix} + S^{-1}\cos k_3 \begin{pmatrix} g_{\mathrm{MF}}^{A\bar{A}} & 0 & 0 \\ 0 & g_{\mathrm{MF}}^{B\bar{B}} & 0 \\ 0 & 0 & g_{\mathrm{MF}}^{C\bar{C}} \end{pmatrix}. \tag{S17}$$

Here,

$$\begin{aligned}
\mu_{\mathrm{MF}}^{A} &= 3J\left[\rho_B - \rho_C - \frac{1+\Delta}{2}(\mathrm{Re}\,\xi_{AB} - \mathrm{Re}\,\zeta_{CA}) - \frac{1-\Delta}{2}(\mathrm{Re}\,\xi_{CA} - \mathrm{Re}\,\zeta_{AB})\right], \\
\mu_{\mathrm{MF}}^{B} &= 3J\left[\rho_A - \rho_C - \frac{1+\Delta}{2}(\mathrm{Re}\,\xi_{AB} - \mathrm{Re}\,\zeta_{BC}) - \frac{1-\Delta}{2}(\mathrm{Re}\,\xi_{BC} - \mathrm{Re}\,\zeta_{AB})\right], \\
\mu_{\mathrm{MF}}^{C} &= 3J\left[-\rho_A - \rho_B + \frac{1+\Delta}{2}(\mathrm{Re}\,\zeta_{BC} + \mathrm{Re}\,\zeta_{CA}) - \frac{1-\Delta}{2}(\mathrm{Re}\,\xi_{BC} + \mathrm{Re}\,\xi_{CA})\right],
\end{aligned}$$

$$\begin{aligned}
t_{\mathrm{MF}}^{AB} &= 3J\left[\xi_{AB} - \frac{1+\Delta}{4}(\rho_A+\rho_B) + \frac{1-\Delta}{8}(\delta_A^* + \delta_B)\right], \\
t_{\mathrm{MF}}^{BC} &= 3J\left[-\xi_{BC} + \frac{1+\Delta}{8}(\delta_B^* + \delta_C) - \frac{1-\Delta}{4}(\rho_B+\rho_C)\right], \\
t_{\mathrm{MF}}^{CA} &= 3J\left[-\xi_{CA} + \frac{1+\Delta}{8}(\delta_C^* + \delta_A) - \frac{1-\Delta}{4}(\rho_C+\rho_A)\right], \\
\Gamma_{\mathrm{MF}}^{A} &= \frac{3J}{2}\left[\frac{1+\Delta}{2}(\xi_{CA} - \zeta_{AB}) + \frac{1-\Delta}{2}(\xi_{AB}^* - \zeta_{CA})\right], \\
\Gamma_{\mathrm{MF}}^{B} &= \frac{3J}{2}\left[\frac{1+\Delta}{2}(\xi_{BC}^* - \zeta_{AB}) + \frac{1-\Delta}{2}(\xi_{AB} - \zeta_{BC})\right], \\
\Gamma_{\mathrm{MF}}^{C} &= \frac{3J}{2}\left[\frac{1+\Delta}{2}(\xi_{BC} - \xi_{CA}^*) - \frac{1-\Delta}{2}(\zeta_{BC} + \zeta_{CA})\right], \\
g_{\mathrm{MF}}^{AB} &= 3J\left[\zeta_{AB} - \frac{1+\Delta}{8}(\delta_A+\delta_B) + \frac{1-\Delta}{4}(\rho_A+\rho_B)\right], \\
g_{\mathrm{MF}}^{BC} &= 3J\left[-\zeta_{BC} + \frac{1+\Delta}{4}(\rho_B+\rho_C) - \frac{1-\Delta}{8}(\delta_B+\delta_C)\right], \\
g_{\mathrm{MF}}^{CA} &= 3J\left[-\zeta_{CA} + \frac{1+\Delta}{4}(\rho_C+\rho_A) - \frac{1-\Delta}{8}(\delta_C+\delta_A)\right],
\end{aligned} \tag{S18}$$

with

$$\begin{aligned}
&\mu_{\mathrm{MF}}^{\bar{A}} = \mu_{\mathrm{MF}}^{B}, \quad \mu_{\mathrm{MF}}^{\bar{B}} = \mu_{\mathrm{MF}}^{C}, \quad \mu_{\mathrm{MF}}^{\bar{C}} = \mu_{\mathrm{MF}}^{A}, \\
&t_{\mathrm{MF}}^{\bar{A}\bar{B}} = t_{\mathrm{MF}}^{BC}, \quad t_{\mathrm{MF}}^{\bar{B}\bar{C}} = t_{\mathrm{MF}}^{CA}, \quad t_{\mathrm{MF}}^{\bar{C}\bar{A}} = t_{\mathrm{MF}}^{AB}, \\
&\Gamma_{\mathrm{MF}}^{\bar{A}} = \Gamma_{\mathrm{MF}}^{B}, \quad \Gamma_{\mathrm{MF}}^{\bar{B}} = \Gamma_{\mathrm{MF}}^{C}, \quad \Gamma_{\mathrm{MF}}^{\bar{C}} = \Gamma_{\mathrm{MF}}^{A}, \\
&g_{\mathrm{MF}}^{\bar{A}\bar{B}} = g_{\mathrm{MF}}^{BC}, \quad g_{\mathrm{MF}}^{\bar{B}\bar{C}} = g_{\mathrm{MF}}^{CA}, \quad g_{\mathrm{MF}}^{\bar{C}\bar{A}} = g_{\mathrm{MF}}^{AB}.
\end{aligned} \tag{S19}$$

are the recombined MF parameters for the intralayer terms. Similarly,

$$\begin{aligned}
t_{\mathrm{MF}}^{A\bar{A}} &= J_c\left[-\frac{1+\Delta}{2}\left(\rho_A+\rho_{\bar{A}}\right) + \frac{1-\Delta}{4}\left(\delta_A^* + \delta_{\bar{A}}\right)\right], \\
t_{\mathrm{MF}}^{B\bar{B}} &= J_c\left[\frac{1+\Delta}{4}\left(\delta_B^* + \delta_{\bar{B}}\right) - \frac{1-\Delta}{2}\left(\rho_B+\rho_{\bar{B}}\right)\right], \\
t_{\mathrm{MF}}^{C\bar{C}} &= J_c\left[\frac{1+\Delta}{4}\left(\delta_C^* + \delta_{\bar{C}}\right) - \frac{1-\Delta}{2}\left(\rho_C+\rho_{\bar{C}}\right)\right],
\end{aligned}$$

$$\begin{aligned}
g_{\mathrm{MF}}^{A\bar{A}} &= J_c\left[-\frac{1+\Delta}{4}\left(\delta_A+\delta_{\bar{A}}\right) + \frac{1-\Delta}{2}\left(\rho_A+\rho_{\bar{A}}\right)\right], \\
g_{\mathrm{MF}}^{B\bar{B}} &= J_c\left[\frac{1+\Delta}{2}\left(\rho_B+\rho_{\bar{B}}\right) - \frac{1-\Delta}{4}\left(\delta_B+\delta_{\bar{B}}\right)\right], \\
g_{\mathrm{MF}}^{C\bar{C}} &= J_c\left[\frac{1+\Delta}{2}\left(\rho_C+\rho_{\bar{C}}\right) - \frac{1-\Delta}{4}\left(\delta_C+\delta_{\bar{C}}\right)\right],
\end{aligned} \tag{S20}$$

are the recombined MF parameters associated with the interlayer coupling.

Figure S3 shows the calculated values of these MF parameters for selected values for $\Delta \leq 1$. We confirmed that all of these MF parameters are real valued; this means that the coefficient matrix in Eq. (S16) has the following form:

$$H_{\mathrm{NLSW}} = \begin{pmatrix} P_{\mathbf{k}} & Q_{\mathbf{k}} \\ Q_{\mathbf{k}} & P_{\mathbf{k}} \end{pmatrix}, \tag{S21}$$

where

$$P_{\mathbf{k}} = \begin{pmatrix} H_{\mathrm{ee},\mathbf{k}} & H_{\mathrm{eo},\mathbf{k}} \\ H_{\mathrm{eo},\mathbf{k}} & H_{\mathrm{oo},\mathbf{k}} \end{pmatrix}, \quad Q_{\mathbf{k}} = \begin{pmatrix} H'_{\mathrm{ee},\mathbf{k}} & H'_{\mathrm{eo},\mathbf{k}} \\ H'_{\mathrm{eo},\mathbf{k}} & H'_{\mathrm{oo},\mathbf{k}} \end{pmatrix} \tag{S22}$$

are 6×6 matrices. This can be diagonalized by a Bogoliubov transformation,

$$\begin{pmatrix} \mathbf{a}_{\mathbf{k}} \\ \bar{\mathbf{a}}_{\mathbf{k}} \\ \mathbf{a}_{-\mathbf{k}}^{\dagger} \\ \bar{\mathbf{a}}_{-\mathbf{k}}^{\dagger} \end{pmatrix} = \begin{pmatrix} U_{\mathbf{k}} & V_{\mathbf{k}} \\ & \\ V_{\mathbf{k}} & U_{\mathbf{k}} \end{pmatrix} \begin{pmatrix} \boldsymbol{\alpha}_{\mathbf{k}} \\ \\ \boldsymbol{\alpha}_{-\mathbf{k}}^{\dagger} \end{pmatrix}, \tag{S23}$$

where $\boldsymbol{\alpha}_{\mathbf{k}}$ ($\boldsymbol{\alpha}_{-\mathbf{k}}^{\dagger}$) is the 6-component vector comprising the annihilation (respectively, the creation) operators of Bogoliubov bosons. The transformation matrices satisfy $U_{\mathbf{k}}^{\mu\kappa} = (U_{-\mathbf{k}}^{\mu\kappa})^*$ and $V_{\mathbf{k}}^{\mu\kappa} = (V_{-\mathbf{k}}^{\mu\kappa})^*$. The poles, $\omega_{\kappa,\mathbf{k}}$, can be obtained as the square-roots of the eigenvalues of $S^2(P_{\mathbf{k}}+Q_{\mathbf{k}})(P_{\mathbf{k}}-Q_{\mathbf{k}})$. As demonstrated in Figs. S2(c) and S2(d), the in-plane dispersion has different characteristics depending on $\tilde{H} \lesssim 3JS$ and $\tilde{H} \gtrsim 3JS$ regarding the band hybridization; the experimental observation in $Ba_3CoSb_2O_9$ at 10.5 T corresponds to the case of $\tilde{H} \lesssim 3JS$.

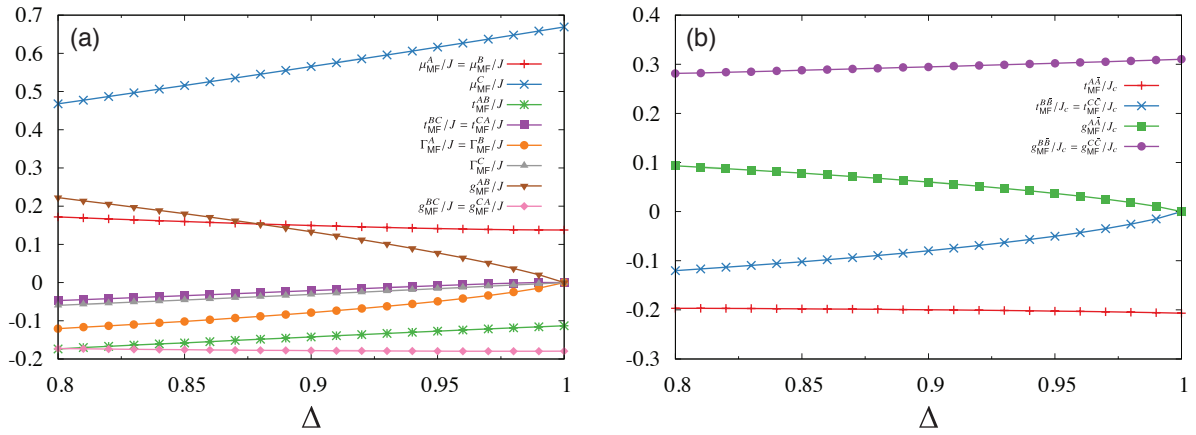

FIG. S3. (a) Δ-dependence of the recombined MF parameters associated with (a) the intra- and (b) the interlayer couplings.

B. Sublattice magnetization

With the phase factors for each sublattice, $c_A = c_B = -c_C = c_{\bar{A}} = -c_{\bar{B}} = c_{\bar{C}} = 1$, we have $S^x_j = c_\mu \tilde{S}^z_j = c_\mu(S - a^\dagger_{\mu,j} a_{\mu,j})$ for site j in sublattice μ. Thus, the reduction of the ordered moment relative to the classical value at site $j \in \mu$ corresponds to the local magnon density:

$$\langle S^x_j \rangle = c_\mu \left(S - \langle a^\dagger_{\mu,j} a_{\mu,j} \rangle \right) = c_\mu \left(S - \frac{1}{N_{\text{u.c.}}} \sum_{\mathbf{k}} \sum_{\kappa} \left| V^{\mu\kappa}_{\mathbf{k}} \right|^2 \right). \tag{S24}$$

C. Dynamical spin structure factor

The dynamical spin structure factor is defined by

$$\begin{aligned} \mathcal{S}^{\alpha\alpha}(\mathbf{q},\omega) &= \int_{-\infty}^{\infty} \frac{dt}{2\pi} e^{i\omega t} \frac{1}{N_{\text{spin}}} \sum_{j,k} e^{-i\mathbf{q}\cdot(\mathbf{r}_j - \mathbf{r}_k)} \left\langle S^\alpha_j(t) S^\alpha_k \right\rangle \\ &= \sum_n \delta(\omega - \omega_n) \left| \langle 0 | S^\alpha_{\mathbf{q}} | n \rangle \right|^2, \end{aligned} \tag{S25}$$

where $|n\rangle$ and ω_n denote the nth excited state and its energy eigenvalue, respectively, and $S^\alpha_{\mathbf{q}} = N^{-1/2}_{\text{spin}} \sum_j S^\alpha_j e^{-i\mathbf{q}\cdot\mathbf{r}_j}$. The longitudinal component is

$$S^x_{\mathbf{q}} = \frac{\sqrt{N_{\text{spin}}}}{3} S \left(\delta_{\mathbf{q},0} + \delta_{\mathbf{q},\mathbf{Q}} + \delta_{\mathbf{q},-\mathbf{Q}} \right) + \delta S^x_{\mathbf{q}}, \tag{S26}$$

with $\mathbf{Q} = (1/3, 1/3, 1)$ and

$$\delta S^x_{\mathbf{q}} = -\sqrt{\frac{1}{N_{\text{spin}}}} \sum_{\mu,\mathbf{k}} c_\mu a^\dagger_{\mu,\mathbf{k}-\mathbf{q}} a_{\mu,\mathbf{k}}, \tag{S27}$$

We truncate the expansions of the transverse components at the lowest order:

$$\begin{aligned} S^y_{\mathbf{q}} &\approx -i \sqrt{\frac{S}{12}} \sum_\mu \left(a_{\mu,\mathbf{q}} - a^\dagger_{\mu,-\mathbf{q}} \right), \\ S^z_{\mathbf{q}} &\approx \sqrt{\frac{S}{12}} \sum_\mu (-c_\mu) \left(a_{\mu,\mathbf{q}} + a^\dagger_{\mu,-\mathbf{q}} \right). \end{aligned} \tag{S28}$$

The transverse components of the dynamical structure factor, $\mathcal{S}_\perp(\mathbf{q},\omega) = \mathcal{S}^{yy}(\mathbf{q},\omega) + \mathcal{S}^{zz}(\mathbf{q},\omega)$, produce the magnon dispersion,

$$\begin{aligned} \mathcal{S}^{yy}(\mathbf{q},\omega) &= \sum_n \delta(\omega - \omega_n) \left| \langle 0 | S^y_{\mathbf{q}} | n \rangle \right|^2 \\ &\approx \frac{S}{12} \sum_\kappa \delta(\omega - \omega_{\kappa,\mathbf{q}}) \left| \sum_\mu \left(U^{\mu\kappa}_{\mathbf{q}} - V^{\mu\kappa}_{\mathbf{q}} \right) \right|^2, \\ \mathcal{S}^{zz}(\mathbf{q},\omega) &= \sum_n \delta(\omega - \omega_n) \left| \langle 0 | S^z_{\mathbf{q}} | n \rangle \right|^2 \\ &\approx \frac{S}{12} \sum_\kappa \delta(\omega - \omega_{\kappa,\mathbf{q}}) \left| \sum_\mu c_\mu \left(U^{\mu\kappa}_{\mathbf{q}} + V^{\mu\kappa}_{\mathbf{q}} \right) \right|^2. \end{aligned} \tag{S29}$$

Meanwhile, $\mathcal{S}^{xx}(\mathbf{q},\omega)$ comprises the elastic contribution and the longitudinal fluctuation,

$$\mathcal{S}_\parallel(\mathbf{q},\omega) = \sum_n \delta(\omega - \omega_n) \left| \langle 0 | \delta S^x_{\mathbf{q}} | n \rangle \right|^2, \tag{S30}$$

which can be evaluated by using Wick's theorem. The result at $T = 0$ is

$$\begin{aligned} \mathcal{S}_\parallel(\mathbf{q},\omega) = \Theta(\omega) N^{-1}_{\text{spin}} \sum_{\mathbf{k}} \sum_{\kappa,\lambda,\mu,\nu} & c_\mu c_\nu \operatorname{Re} A_{\mu\nu;\kappa\lambda}(\mathbf{k};\mathbf{q}) \\ & \times \delta(\omega - \omega_{\kappa,-\mathbf{k}+\mathbf{q}} - \omega_{\lambda,\mathbf{k}}), \end{aligned} \tag{S31}$$

where

$$\begin{aligned} A_{\mu\nu;\kappa\lambda}(\mathbf{k};\mathbf{q}) = \frac{1}{2} & \left[\left(U^{\mu\kappa}_{\mathbf{k}-\mathbf{q}} \right)^* V^{\mu\lambda}_{\mathbf{k}} + \left(V^{\mu\kappa}_{\mathbf{k}-\mathbf{q}} \right)^* U^{\mu\lambda}_{\mathbf{k}} \right] \\ & \times \left[U^{\nu\kappa}_{\mathbf{k}-\mathbf{q}} \left(V^{\nu\lambda}_{\mathbf{k}} \right)^* + V^{\nu\kappa}_{\mathbf{k}-\mathbf{q}} \left(U^{\nu\lambda}_{\mathbf{k}} \right)^* \right]. \end{aligned} \tag{S32}$$